Direct radiative effect of mineral dust and volcanic aerosols in a simple aerosol climate model

Karen M. Shell[1,2] and Richard C. J. Somerville[1]

[1]   Airborne mineral dust can influence the climate by altering the radiative properties of the atmosphere, but the magnitude of the effect is uncertain. An idealized global model is developed to study the dust-climate system. The model determines the dust longwave and shortwave direct radiative forcing, as well as the resulting temperature changes, based on the specified dust distribution, height, and optical properties. Comparisons with observations and general circulation results indicate that the model produces realistic results for the present-day dust distribution as well as for volcanic aerosols. Although the model includes many simplifications, it can still provide insight into dust-climate system behavior. Recent observations suggest that dust may absorb less solar radiation than previously thought. Experiments with the model suggest that previous studies which used more absorbing dust may be underestimating the effect of dust. Increasing the solar single scattering albedo value from 0.85 to 0.97, corresponding to recent measurements, more than doubles the modeled global average top-of-the-atmosphere (TOA) shortwave direct forcing for the present-day dust distribution, while the surface shortwave forcing is halved. The corresponding temperature decreases are larger for the larger single scattering albedo, and the latent and sensible heat fluxes decreases are smaller. The dust forcing and climate response are approximately linear with respect to optical depth. However, the relationship depends on the relative magnitudes of shortwave versus longwave TOA forcing. Thus the net TOA forcing alone does not determine the steady state climate response.

Citation: Shell, K. M., and R. C. J. Somerville (2007), Direct radiative effect of mineral dust and volcanic aerosols in a simple aerosol climate model, *J. Geophys. Res.*, *112*, D03205, doi:10.1029/2006JD007197.

1. Introduction

[2]   Mineral, or desert, dust is one of the major aerosol species, comprising about a third of the total global aerosol optical thickness [*Tegen et al.*, 1997], yet the effect of dust on the climate system is poorly constrained. Airborne dust both reflects and absorbs solar radiation. It also absorbs and emits infrared (IR) radiation, thus contributing to the greenhouse effect. However, the current net direct radiative effect of dust is unclear because the present-day atmospheric distribution and optical properties of dust are highly uncertain. For example, *Myhre and Stordal* [2001] conclude that the range of globally averaged top-of-atmosphere (TOA) forcing lies between -1.4 and $+1.0$ W/m^2. Furthermore, the effect that dust will have on the future climate is unknown, since estimates of future changes in atmospheric dust loading differ both in magnitude and sign [*Mahowald and Luo*, 2003; *Tegen et al.*, 2004a; *Mahowald et al.*, 2004; *Tegen et al.*, 2004b].

[3]   The TOA forcing depends on the surface albedo and properties of the atmospheric column as well as the dust optical properties. Locally, the TOA effect can be either positive or negative [*Claquin et al.*, 1998; *Liao and Seinfeld*, 1998]. Over dark surfaces (e.g., ocean) dust increases the apparent reflectance of the Earth. This reduced shortwave usually dominates the increased longwave, leading to a net cooling of the column. Over bright surfaces, such as snow or desert, or cloud-covered surfaces, absorption of solar radiation dominates over scattering, causing a net TOA warming, unless the reflectivity of dust is very high [e.g., *Weaver et al.*, 2002]. Global calculations indicate that the (positive) longwave and (negative) shortwave forcings tend to cancel, so that the globally averaged TOA forcing is close to zero [*Tegen et al.*, 1996]. However, the sign of this global mean forcing is heavily dependent on the specific optical properties of the dust [*Miller and Tegen*, 1999; *Myhre and Stordal*, 2001].

[4]   Even though the TOA forcing is often small, the surface forcing can be relatively large. Both solar absorption and reflection within the atmosphere tend to cool the surface, because less solar radiation reaches the surface. While an increased longwave flux (due to the dust "greenhouse effect") somewhat balances the cooling, the net result is normally large and negative.

---

[1]Scripps Institution of Oceanography, University of California, San Diego, La Jolla, California, USA.
[2]Now at College of Oceanic and Atmospheric Sciences, Oregon State University, Corvallis, Oregon, USA.

Table 1. Annual and Global Average Shortwave, Longwave, and Net Dust Forcing From Radiative Transfer Model Results[a]

Model	TOA SW	TOA LW	TOA net	Surface SW	Surface LW	Surface Net
Tegen et al. [1996]			+0.14			
Miller and Tegen [1998]			−0.1			−2.1
Woodward [2001]	−0.16	0.23	0.07	−1.22	0.40	−0.82
Myhre and Stordal [2001] 1	−0.02	0.41	0.39			
Myhre and Stordal [2001] 2	−0.53	0.13	−0.40			
Jacobson [2001]			−0.14			−0.85
Perlwitz et al. [2001]	−0.5	0.1	−0.4	−2.1	0.4	−1.7
Claquin et al. [2003]			−1.2			
Miller et al. [2004]	−0.33	0.15	−0.18	−1.82	0.18	−1.64
Miller et al. [2004] (0.9 x ω)	0.61	0.15	0.76	−2.65	0.18	−2.47
Miller et al. [2004] (1.1 x ω)	−0.96	0.14	−0.82	−1.24	0.17	−1.07
Miller et al. [2006]			−0.39			−0.82
Yoshioka et al. [2006]	−0.92	0.31	−0.60	−1.59	1.13	−0.46
This work ($\omega = 0.97$)	−0.73	0.23	−0.49	−1.34	0.37	−0.97
This work ($\omega = 0.85$)	−0.31	0.23	−0.07	−2.70	0.37	−2.33

[a]Forcing given in W/m^2. *Myhre and Stordal* [2001] use two different dust distributions: (1) *Koepke et al.* [1997] and (2) *Tegen and Fung* [1995]. Results from this work are shown for two different shortwave (SW) single scattering albedos. The longwave (LW) forcings for these two cases are identical.

[5] Since the direct radiative effect of dust varies temporally and spatially and is thus difficult to measure, the globally averaged effect has been explored using radiative transfer models with specified dust distributions [e.g., *Tegen et al.*, 1996; *Woodward*, 2001; *Myhre and Stordal*, 2001]. The results from these and other studies are summarized in Table 1 and show both positive and negative net TOA forcing.

[6] The heating changes can in turn cause dynamical changes in atmospheric circulation and stability. For example, increased absorption of solar radiation within the atmosphere results in atmospheric warming and surface cooling [*Carlson and Benjamin*, 1980; *Tegen et al.*, 1996]. This redistribution of heating within the column affects the stability of the atmosphere, with implications for convection, latent heat transport, cloudiness, and precipitation. *Miller and Tegen* [1998] use an atmospheric GCM with an ocean mixed layer to calculate heating rates using the dust distribution from *Tegen and Fung* [1994]. They find a surface temperature reduction of 1 K beneath dust clouds. The effect on surface temperature is largest outside convecting regions. In addition, the hydrological cycle alters in response to changes in sea surface temperature; precipitation decreases under dust clouds due to reduced evaporation. This reduced hydrological cycle is consistent with earlier work [*Coakley and Cess*, 1985] showing decreased precipitation in response to reduced solar radiative heating of the surface.

[7] Previous modeling work on dust forcing and the climate response has concentrated on a few scenarios run in GCM experiments. Two drawbacks to these studies are excessive computational requirements and difficulty in interpreting results. We have developed a simple energy balance model to explore the direct radiative effect of dust and aerosols on the climate system for a wide variety of scenarios. The model is capable of computing over 800 steady state solutions in a day on a workstation, whereas a similar number of calculations in a GCM would require years of supercomputer time. Because of its simplicity, our model can also provide a more readily accessible conceptual understanding of results. This insight can then be tested in more complex models, or the results can be used to drive parameter selection for GCM experiments.

[8] In this paper, we build on the model described by *Shell and Somerville* [2005] to include the direct radiative effects of aerosols. Although the original purpose of the model was to study dust, the basic model is more generally applicable to other aerosols as well, assuming the aerosol distribution and optical properties are modified appropriately. To evaluate the model, we compare the response of the model to a volcanic aerosol distribution from the Pinatubo eruption to observations and GCM results. We then use the model to estimate the direct radiative forcing and resulting temperature change for the present-day dust distribution and determine the dependence of these results on the shortwave single scattering albedo, which is presently uncertain. We also examine the dependence of the climate response to variations in dust concentration.

[9] *Shell and Somerville* [2007] use this calibrated model to perform sensitivity studies to analyze the climate sensitivity to dust optical properties and height. These results will suggest the areas of largest uncertainty in the direct radiative effect of dust on climate. Future research can then focus on refining the dust optical properties associated with the largest uncertainties in the climate response to dust.

2. Model Description

[10] The simple model consists of a longitudinally averaged atmosphere layer above a surface layer, which represents the combined influences of ocean and land. Both layers are composed of the same number of grid points from pole to pole, so that different latitude bands are resolved. The model determines steady state temperatures of the atmosphere (T_a) and surface (T_s) for each latitude (ϕ) such that the different heating and cooling mechanisms balance:

$$C_a \frac{\partial T_a}{\partial t} = 0 = S_a + I_a + F_s + F_l + D_a \qquad (1)$$

$$C_s \frac{\partial T_s}{\partial t} = 0 = S_s + I_s - F_s - F_l + D_s \qquad (2)$$

where C is the heat capacity, t is time, S is the net solar (shortwave) heating, I is the net infrared (longwave) heating, F_s and F_l are the sensible and latent heat fluxes
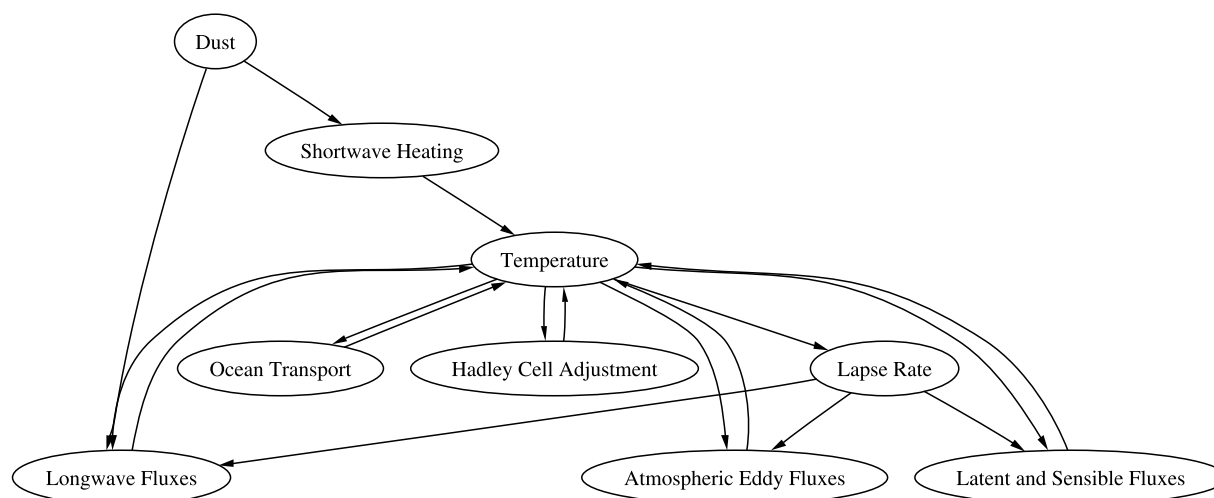
Figure 1. Model components. The primary model variables are atmospheric and surface temperatures. Dust influences the longwave and shortwave radiative budgets. The steady state temperature is determined by the balance of the radiative, dynamic, and surface-atmosphere fluxes, which are in turn based on the temperatures, as well as intermediate variables, such as the atmospheric lapse rate.

from the surface to the atmosphere, and D is the rearrangement of heat due to dynamical effects. The subscripts $_a$ and $_s$ refer to atmospheric terms and surface terms respectively. Figure 1 illustrates the main components of the model.

[11] Although the model includes a single atmospheric layer, it does approximate the vertical structure of the atmosphere with an explicitly calculated, latitudinally varying lapse rate. In the tropics, the lapse rate corresponds to the moist adiabatic lapse rate based on the boundary layer temperature and the specified relative humidity at the equator. At higher latitudes, the lapse rate is set to the critical lapse rate for baroclinic adjustment [*Stone*, 1978]. This prognostic lapse rate allows the use of temperatures at different heights in the atmosphere, such as the boundary layer temperature.

[12] In the aerosol-free version of the model, we specify atmospheric shortwave absorptivity, reflectivity, and transmissivity, as well as surface albedo, as a function of latitude. Clouds are implicitly included in these atmospheric optical properties, but they do not vary with the climate system, so the model does not include any cloud feedbacks. Allowing for multiple reflections between the surface and the atmosphere, the model calculates the surface and atmospheric heating. The aerosol-free longwave budget includes emission and absorption from the surface and atmosphere. The atmospheric terms are influenced by a latitudinally varying emissivity, which depends on the boundary layer temperature. Thus the longwave calculation includes a simple water vapor feedback parameterization.

[13] The latent and sensible heat fluxes are calculated by the bulk formulas, assuming a constant boundary layer relative humidity. The model determines the meridional transport of heat via three mechanisms: ocean transport, midlatitude atmospheric eddies, and the Hadley circulation. Ocean transport is modeled as a modified diffusive process [*Thompson and Pollard*, 1997], where the transport depends on the meridional temperature gradient as well as a latitudinally varying diffusivity. The atmospheric eddy transport

is based on the work by *Stone* [1974] and is related to both the local meridional temperature gradient and the tropospheric lapse rate. This formulation allows for feedbacks between the lapse rate and the meridional heat flux. To determine the heat transport by the Hadley cell, we implement the inviscid analytic model of *Held and Hou* [1980], which assumes angular momentum conservation and thus limits meridional temperature gradients in the tropics. The Hadley cell parameterization affects tropical atmospheric temperatures within the Hadley cell, while the eddy transport parameterization is used at all latitudes, though its magnitude peaks in the midlatitudes. Full descriptions of these heating terms are included by *Shell and Somerville* [2005].

[14] The model is an energy balance model similar to those used by *Budyko* [1969] and *Sellers* [1969]. However, this model is notable in that it treats the surface and the atmosphere separately. This separation is necessary to resolve the differing effects of dust on the surface and atmosphere. In addition, the meridional transport of heat is further divided in the atmosphere into transport by the Hadley circulation and by midlatitude eddies. The separation of heat transports allows for more detailed study of dynamical feedbacks and responses to aerosol forcing. Finally, the prognostic lapse rate allows for feedbacks not normally included in simple energy balance models. Studies with the dust-free model [*Shell and Somerville*, 2005] indicate that the inclusion of an interactive lapse rate has a significant impact on the sensitivity of the model.

[15] The model produces a realistic steady state climate. Although the simple treatment of processes such as water vapor transport result in differences between the modeled and observed surface temperatures at some latitudes, the global average temperature and energy budget values are within the uncertainty of observations. The modeled climate sensitivity to changes in radiative forcing, as determined from a 2% solar constant increase experiment, is lower that the *Intergovernmental Panel on Climate Change (IPCC)* [2001] climate sensitivity estimate (1.5 to 4.5 K). This

reduced sensitivity (1.0 K for surface temperature and 1.3 K for atmospheric temperature) is related to a too-weak water vapor (positive) feedback, a too-strong lapse rate (negative) feedback, and the lack of any solar radiation feedbacks (such as the positive ice albedo feedback). Thus the magnitude of climate responses to aerosol radiative forcing obtained by our model may be too small. However, climate sensitivity to absorbing aerosols such as dust may be different from sensitivity to the solar constant or greenhouse gases [*Hansen et al.*, 1997]. For example, the ice albedo feedback may not be relevant for dust forcing, which may be concentrated at lower latitudes. In any case, the point of our model is not to produce the definitive answer to the question of the magnitude of the climate response to dust forcing, which is a question more suited for general circulation models. Instead, we are interested in how different climate components (e.g., the temperature and the latent heat flux) interact in response to dust, and which factors are important in determining the climate response.

[16] The model calculates the longwave and shortwave aerosol direct forcing based on the specified latitudinally varying aerosol concentration and global average optical properties. For the purposes of this study, we define the radiative forcing to be the difference between the net instantaneous radiative heating in the version of the model with the aerosol and the aerosol-free version of the model. Thus the forcing corresponds to the total effect of the particular aerosol, not just the anthropogenic component, though this anthropogenic forcing could be estimated by comparing model results from natural and total (natural plus anthropogenic) dust simulations.

[17] To determine the direct shortwave effect of the aerosol, we recalculate the atmospheric radiative properties (absorptivity A and A^*, reflectivity R and R^*, and transmissivity T and T^*) to light from above (terms with no asterisks) and from below (terms with asterisks). We start by dividing the atmosphere into two "clean" layers separated by the aerosol layer, which is approximated as a δ-Eddington layer [*Joseph et al.*, 1976]. We specify a broadband single scattering albedo (ω), asymmetry parameter (g), and height of the aerosol layer. The optical depth (τ) is linearly related to the aerosol column loading by the specific extinction cross section (B). All three (ω, g, and B) are constant with respect to time and latitude. The specified atmospheric pressure at the height of the aerosol layer determines how much atmospheric reflection of solar radiation occurs above the aerosol layer and how much occurs below it, corresponding to the distribution of clouds (or other radiatively active particles) above and below the dust layer. We can adjust this shortwave pressure to account for different vertical distributions of optically active constituents (i.e., clouds) within the atmosphere. We then use the adding method [*Liou*, 2002] to combine the dust layer with the layers of atmosphere above and below it. The auxiliary material contains a full description of all the aerosol forcing calculations.[1]

[18] The shortwave radiation budget does not depend on the modeled climate state. It is entirely specified by externally applied parameters, and clouds are specified. The

model includes no feedbacks between the climate and the shortwave budget, such as the semidirect aerosol effect on clouds [*Hansen et al.*, 1997] or the modification of clouds by aerosols acting as condensation nuclei (the indirect effect). However, clouds are extremely difficult to model, even in general circulation models, and the net result of the indirect effect is still unclear. We have chosen to omit any shortwave radiative feedbacks, focusing instead on other feedbacks, such as longwave radiation feedbacks and latent and sensible heating feedbacks, which are better resolved by our model.

[19] To determine the direct longwave effect of the aerosol, we use the simple model of infrared forcing developed by *Markowicz et al.* [2003]. This model assumes the effect of the aerosol is in the atmospheric window (8–12 μm) and that no gaseous or cloud-related absorption occurs in the window. In addition, the aerosol layer is treated as isothermal, and multiple scattering within the layer is neglected. The longwave forcing is determined from the aerosol temperature, which is based on the specified aerosol layer height, and the broadband single scattering albedo, asymmetry parameter, and optical depth corresponding to the longwave part of the spectrum.

[20] While the shortwave radiative aerosol forcing is based solely on a given set of specified values, the longwave forcing depends on the temperature of the atmosphere and the prognostic lapse rate. Thus it can vary as the climate changes, allowing for feedback between the aerosol forcing and climate state. However, this model does not include the effects of clouds on the longwave forcing, which have been shown to decrease the forcing in one-dimensional radiative transfer models [*Liao and Seinfeld*, 1998].

[21] These parameterizations were chosen to be consistent with the overall complexity and uses of the model; we are interested in the general behavior of the climate system rather than the specific magnitude of the response. For example, we assume a gamma particle size distribution [*Lacis and Mishchenko*, 1995] everywhere, which allows us to linearly relate the optical depth to the column loading. However, for mineral aerosols, we expect the distribution to change during transport [*Tegan et al.*, 2002, Figure 4]. Thus the relationship between column mass and optical depth should vary regionally, as they do in GCMs with different dust size bins [e.g., *Tegen and Fung*, 1994].

[22] In addition, we use a single broadband calculation for each radiative calculation (i.e., shortwave and longwave). Aerosol optical properties, however, vary with spectral wavelength. (See, for example, Figure 1 of *Sokolik and Toon* [1996].) Our ω, g, and B values are representative broadband values, such that the resulting shortwave radiative effect should be similar to that calculated by a more spectrally resolved radiative transfer model. Thus the values do not correspond to a particular wavelength. Since the bulk single scatter albedo tends to be similar to the value corresponding to the predominant particle size [e.g., *Miller et al.*, 2004], we compare our value to the value at this size mode when bulk values are not available. We neglect the variation of radiative properties with wavelength, which is included in GCMs, in order to maintain the conceptual simplicity and computational speed of the model.
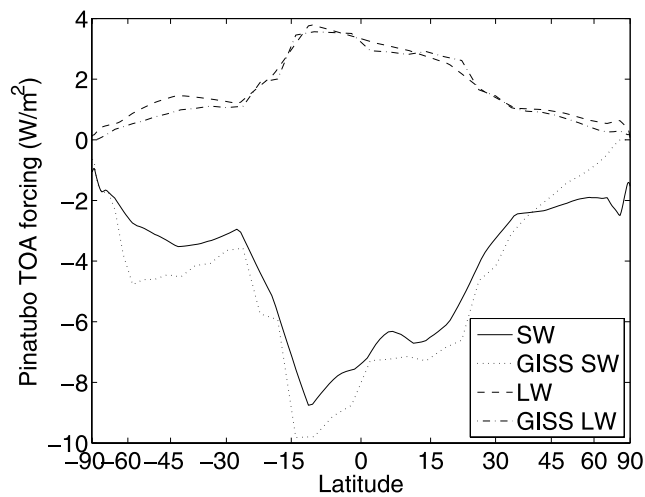
[23] In addition to the broadband approximation, we also assume the optical properties are constant with respect to

---

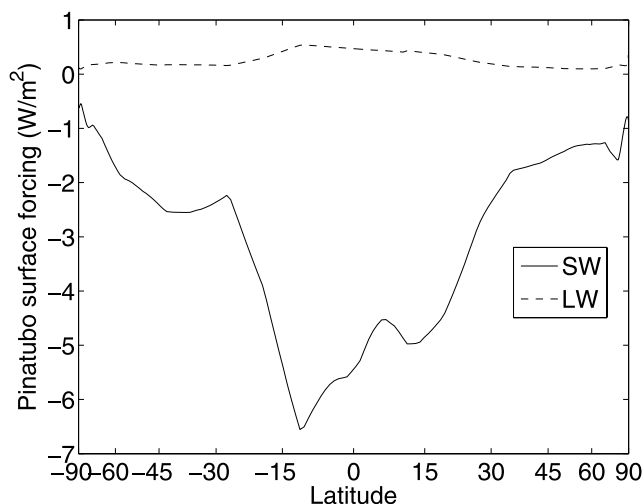[1]Auxiliary materials are available in the HTML. doi:10.1029/2006JD007197.
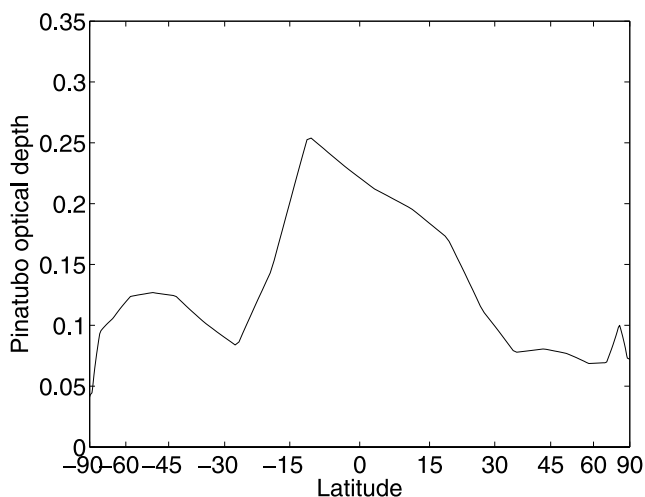
Figure 2. Imposed optical depth of Pinatubo aerosol at 550 nm for November 1991 [*Sato et al.*, 1993].

Figure 4. Modeled Pinatubo surface shortwave and long-wave forcing.

location and time. In the case of mineral aerosols, actual values vary based on mineralogy, size, shape, and weathering processes. Different sources produce dust particles with different optical properties [*Sokolik et al.*, 1993], and once the dust is airborne, these properties change with time as a result of different particle lifetimes [*Tegen and Lacis*, 1996] and interaction with other aerosols [*Trochkine et al.*, 2003]. There is no single set of values that can describe all dust. In fact, this is part of the motivation for the development of this model. If dust optical properties were the same at all times and locations, a spectrally dependent radiative transfer model could be run to generate a fairly accurate dust effect. However, given the uncertainty in dust optical properties, it is useful to explore the relationship between optical properties and the radiative effect. Although any individual

steady state of our model cannot correspond to an actual dust case, we can bracket different cases. By examining the climate system behavior for a wide variety of case, we can study how different processes within the climate respond to dust and how the climate response changes as we alter various parameters.

3. Evaluation of Model With Pinatubo Aerosol Scenario

[24] In June 1991, the Mount Pinatubo volcano in the Philippines erupted, injecting 20 Mt of SO_2 into the atmosphere [*Bluth et al.*, 1992]. The SO_2 converted to sulfate aerosol within a few weeks, altering the radiation budget and climate of the Earth. Since the eruption occurred in an era of satellites, aircraft observing platforms, and global observing networks, much data was collected related to this large eruption, including estimates of TOA forcing and observations of resulting temperature changes. In addition, many models have been used to simulate and study the climatic effects of the eruption.

[25] We perform a Pinatubo experiment with our simple model to test the model's ability to produce a realistic climate response to an imposed aerosol distribution, comparing the instantaneous forcing and temperature with observations and other model results. We use the zonal and monthly average shortwave aerosol optical depth for November 1991 (Figure 2) from the updated stratospheric aerosol data set of *Sato et al.* [1993] used by *Hansen et al.* [2002]. Instead of the dust optical properties listed in Table S1 in the auxiliary material, we use optical properties more representative of volcanic aerosols. We specify the shortwave dust pressure to be 50 mbar. The longwave dust height is 15 km, ω is 1 (entirely scattering), and $g = 0.84$. We assume the longwave optical depth is 0.15 of the shortwave optical depth, $\omega_{IR} = 0.15$, and $g_{IR} = 0.4$.

[26] Figures 3 and 4 show the instantaneous forcing for this Pinatubo aerosol distribution. The TOA forcings are compared with TOA forcings [*Oman et al.*, 2005; *Stenchikov et al.*, 1998] calculated using the *Sato et al.*

Figure 3. Modeled November 1991 Pinatubo TOA short-wave (SW) and longwave (LW) forcing compared with results from the GISS E model [*Oman et al.*, 2005; *Stenchikov et al.*, 1998].

Table 2. Changes in Global Averages Due to the Pinatubo Aerosol

Variable	Difference
Surface temperature, K	−0.55
Atmospheric temperature, K	−0.70
TOA shortwave heating, W/m^2	−4.31
TOA longwave heating, W/m^2	1.80
Surface shortwave heating, W/m^2	−3.14
Surface longwave heating, W/m^2	0.26
Latent heating, W/m^2	−2.90
Sensible heating, W/m^2	−0.75

[1993] aerosol data set in the GISS model E. Our model uses the same aerosol optical depth, but its simpler radiative calculation can be performed in a fraction of the time. The ability of this simple model to produce very similar TOA forcings indicates that it can be a useful tool in studying the effects of aerosols.

[27] Table 2 shows the global average instantaneous Pinatubo aerosol forcing. The TOA shortwave forcing is −4.3 W/m^2, while the longwave forcing is 1.8 W/m^2. *Kirchner et al.* [1999], using the ECHAM4 GCM, estimate a maximum TOA shortwave "forcing with response" (difference between model results with the volcanic aerosols and without) of more than −4.0 W/m^2 and a longwave forcing of 1.5 W/m^2, resulting in a net 2.5 W/m^2 forcing. *Hansen et al.* [2002] obtain a peak global mean net forcing of about −3 W/m^2 in the GISS SI2000 model (note that this value is at the top of the troposphere, rather than TOA). Our model TOA results are thus within the range of realistic radiative changes.

[28] At the surface, the global average instantaneous shortwave forcing is −3.1 W/m^2, and the longwave forcing is 0.3 W/m^2. With the ECHAM4 GCM, *Kirchner et al.* [1999] obtain a global average surface shortwave radiative "forcing with response" of about −3 W/m^2 for November 1991. The longwave flux change is small, around 0.5 W/m^2 over land. Since the sea surface temperature was held constant, global average longwave flux changes over the ocean vanish. Our longwave surface flux is instantaneous and therefore includes no adjustments by the climate system in response to the forcing. Given these constraints, our surface radiative changes are also reasonable.

[29] Figure 5 shows the resulting equilibrium temperature change in response to the Pinatubo aerosol forcing. The atmosphere cools by about 0.7 K, while the surface cools by 0.5 K. The atmosphere cools the most in the tropics (except for the slight increase at 45 degrees south, corresponding to the forcing peak there), with the cooling otherwise decreasing monotonically toward the poles. The surface temperature decrease also peaks at the equator, but there are much larger maxima around 45 to 60 degrees north and south. These are related to sharp boundaries in different model components, such as the transition point from a moist adiabatic lapse rate to a baroclinic lapse rate or a change in the latitudinal extent of the region where latent heat flux occurs (the flux is constrained to be positive, so high latitudes generally do not have a latent heat flux from the surface to the atmosphere). These sharp transitions are artifacts of the model, and they are emphasized in this

experiment due to the large magnitude of the forcing. Smaller forcings result in smoother distributions. In comparing the model with observed temperature changes and other model results, we concentrate on global rather than latitudinal averages. Table 2 shows the global average temperature changes.

[30] The global average surface temperature cools by 0.55 K, though the peaks have increased the magnitude of the change. The atmospheric temperature decreases by 0.7 K. *Kirchner et al.* [1999] obtain a maximum global average surface air temperature cooling of almost 0.4 K in their GCM experiment. Observations show a maximum cooling of 0.5 K [*Jones and Briffa*, 1992; *Dutton and Christy*, 1992]. These observations and GCM results correspond to a transitory response to a changing radiative forcing; the maximum forcing occurs in winter of 1991, but the maximum temperature response is delayed until fall of 1992. Our model temperatures represent the equilibrium climate response to a constant forcing. Thus, as expected, our model demonstrates a stronger temperature change.

[31] We see significant changes in the latent and sensible heat fluxes as a result of the imposed volcanic aerosol forcing (Figure 6). The latent heat flux difference peaks in the subtropics, while the sensible heat flux change varies little with latitude. The global average latent heat flux decreases by almost 3 W/m^2 (3.7%), and the sensible heat flux decreases by 0.75 W/m^2 (3.4%). *Robock and Liu* [1994] find reduced precipitation following eruptions similar to Agung (1963) and El Chichon (1982) in GISS GCM transient simulations [*Hansen et al.*, 1988]. The average maximum reduction is about 0.05 mm/day (about 1.5%). This reduction is not as large as our reduction. However, the Pinatubo optical depth was 1.7 times larger than the El Chichon optical depth [*Dutton and Christy*, 1992]. *Soden et al.* [2002] obtain a maximum global water vapor reduction of about 0.75 mm (3%) in a GCM simulation of the Pinatubo eruption, closer to our model results. In addition, both the *Robock and Liu* [1994] and *Soden et al.* [2002] results are transient responses, while our model
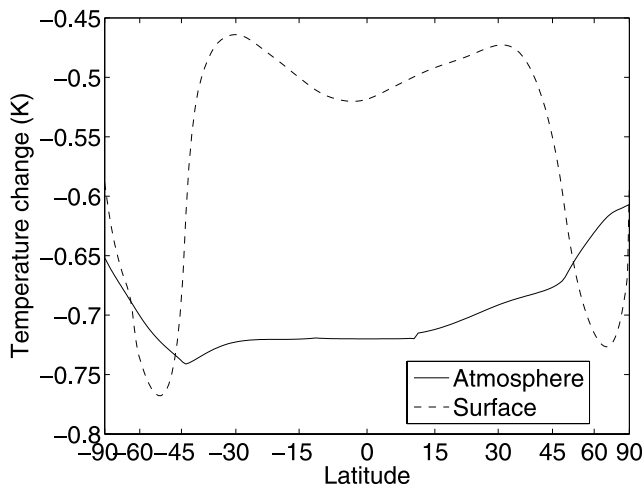
Figure 5. Atmospheric and surface temperature change caused by Pinatubo aerosol.
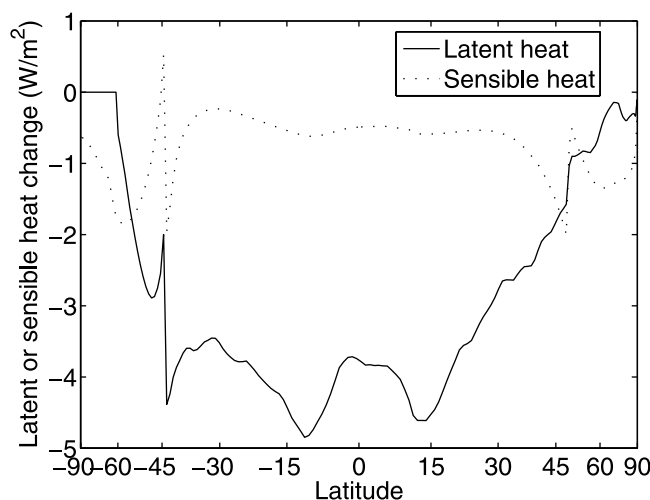
Figure 6. Change in latent and sensible heat fluxes caused by Pinatubo aerosol.

produces the equilibrium response. Thus our larger hydrological cycle change is very reasonable.

[32] Our model does not produce some known climate responses to volcanic eruptions, such as Northern Hemisphere winter warming [*Robock and Mao*, 1995]. This warming is caused by a strengthening of the stratospheric polar vortex, resulting in altered tropospheric circulation [*Kirchner et al.*, 1999]; these dynamical processes are not included in our model. In addition, the magnitude of the forcing is larger than our model can deal with smoothly, leading to unrealistic results at high latitudes. However, the model does produce realistic global average forcing, temperature, and hydrological cycle changes. Thus our simple model reproduces most of the major climate changes in response to the Pinatubo eruption within the uncertainty of the observations and GCM model results.

4. Direct Radiative Effect of Mineral Dust on Climate

[33] Since the results from the Pinatubo simulation indicate that the simple model can be a useful tool for studying the effects of aerosols, we turn our attention to the original purpose of the model, studying the effects of mineral dust. Our model determines the steady state climate forcing and temperature response for a particular dust distribution. Table S1 in the auxiliary material summarizes the variables and default specified parameters for the dust module of our model.

[34] We begin by studying the detailed climate response for our default dust distribution, the present-day climatological concentration from *Tegen and Lacis* [1996] and *Tegen et al.* [1997], which is derived from a tracer transport model [*Tegen and Fung*, 1994] including the uplift, transport, and deposition of dust. This distribution corresponds to a source strength of 1200 Tg/yr and a mean load of 36 mg m^{-2} (18 Tg). In comparison, a compilation of recent dust statistics by *Zender et al.* [2004] gives an emissions range of 1000–2150 Tg/yr and a load range of 8–36 Tg.

Figure 7 shows the reflectivity, absorptivity, and optical depth of the dust layer. The resulting globally averaged optical depth is 0.033. Table 3 summarizes global average changes in the model when compared to the dust-free steady state, described by *Shell and Somerville* [2005].

4.1. Climate Forcing

[35] We first obtain the instantaneous forcing due to dust. Starting with the dust-free model, we recalculated the radiative heating and cooling using the new shortwave optical properties for a dusty atmosphere and the longwave forcing for a dust layer while holding the temperature constant. These calculations exclude any climate feedbacks, which we study later.

[36] For this section, we use two different values for the broadband shortwave single scattering albedo, ω, the ratio of reflected radiation to the total reflected and absorbed radiation. Although observations may indicate a particular single scattering albedo value at a particular time and place, the spatial and temporal variation of ω makes it difficult to determine a "representative" value, if such an approximation is possible. Even dust clouds with the same mineralogy result in different single scattering albedos for different size distributions. Figure 1 of *Sokolik and Toon* [1996] shows that the single scattering albedo varies significantly based on the assumed size distribution and mineralogy. While they use $\omega = 0.85$ as a representative value, some recent observational studies [e.g., *Wang et al.*, 2003; *Kaufman et al.*, 2001; *Christopher et al.*, 2003; *Haywood et al.*, 2003; *Clarke et al.*, 2004] suggest much higher values, corresponding to more reflective, as opposed to absorptive, dust. Since some of the previous estimates of global average dust forcing correspond to a lower ω value, we show model results for $\omega = 0.85$ to verify that our model produces reasonable results and study its sensitivity to this parameter. However, for our estimate of the climatic effect of dust, we use $\omega = 0.97$, since recent literature suggests this is a more
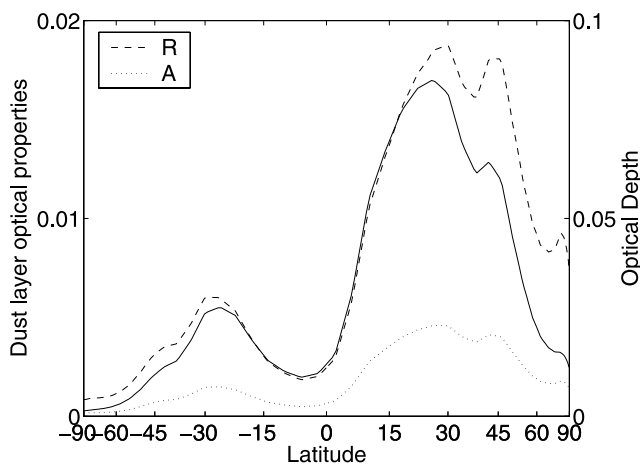
Figure 7. Shortwave reflectivity (dashed), absorptivity (dotted), and optical depth (solid) of the dust layer. The transmissivity can be obtained by subtracting the sum of the reflectivity and absorptivity values from 1.

Table 3. Changes in Global Averages Due to Dust[a]

Variable	Difference ($\omega = 0.97$)	Difference ($\omega = 0.85$)
Surface temperature, K	−0.12	−0.08
Atmospheric temperature, K	−0.13	−0.01
TOA shortwave heating, W/m^2	−0.73	−0.30
TOA longwave heating, W/m^2	0.73	0.30
Latent heating, W/m^2	−0.74	−1.13
Sensible heating, W/m^2	−0.28	−0.74
Planetary albedo	0.002	0.001
Solar radiation absorbed by atmosphere, W/m^2	0.62	2.40
Solar radiation absorbed by surface, W/m^2	−1.34	−2.70
LW emitted from atmosphere to surface, W/m^2	−0.68	0.01
LW emitted by surface, W/m^2	−0.63	−0.46
LW absorbed by atmosphere, W/m^2	−0.82	−0.42
LW emitted by atmosphere, W/m^2	−1.36	−0.02
LW absorbed-emitted by dust layer, W/m^2	−0.14	−0.14
LW emitted by dust layer to surface, W/m^2	0.37	0.37

[a]Longwave emission and absorption by the dust-free atmosphere and dust layer are listed separately. Decreased emissions by the atmosphere and surface are warming effects.

realistic value. Results from later GCM studies [e.g., *Miller et al.*, 2006; *Yoshioka et al.*, 2006] will correspond more closely to this value as well. *Shell and Somerville* [2007] more fully explore the climate's dependence on various specified parameters, including the shortwave single scattering albedo.

[37] Figure 8 shows the surface, atmospheric, and TOA instantaneous dust forcing. The longwave forcing warms the surface, while the shortwave forcing cools the surface. The net effect is one of cooling, since the shortwave cooling dominates. The magnitude of the shortwave cooling is much larger in the $\omega = 0.85$ case (corresponding to more absorptive dust) than in the $\omega = 0.97$ case. In the atmosphere, the shortwave again dominates the longwave, but the signs of the forcings are reversed so that the atmosphere experiences a net warming. The atmospheric warming is less than the surface cooling, though only slightly less in the $\omega = 0.85$ case, where the two are similar in magnitude. In both cases, the shortwave TOA effect is one of cooling, corresponding to an increase in the global average TOA albedo. The TOA longwave effect is warming. While the shortwave TOA forcing is much smaller in magnitude than the surface forcing, it is still larger than the TOA longwave forcing, resulting in a net planetary cooling. For the $\omega = 0.97$ case, the net TOA forcing is always negative. However, in the $\omega = 0.85$ case, the shortwave (and net) TOA forcing is actually positive at high latitudes. This warming is a result of the high surface albedo in these regions. The dust absorbs reflected sunlight which would otherwise be lost to space, resulting in a local decrease of TOA albedo. The TOA shortwave forcing is thus over twice as large for the $\omega = 0.97$ case than the $\omega = 0.85$ case. The global average longwave forcings are the same for both cases. Since the shortwave forcings are quite different, the net forcings are also different between the two cases, with TOA cooling stronger in the $\omega = 0.97$ case, and the surface cooling stronger in the $\omega = 0.85$ case. These results suggest that calculations of dust forcing derived using older optical property values may be underestimating the effect of dust, if dust is, in fact, more reflective than originally thought.

[38] Table 1 compares our globally averaged results with those obtained from other models. The longwave and shortwave forcings are within the range obtained by other investigations. Indeed, differences between previous model results are as large as differences between our model and others. Given the simplicity of the model, the similar results indicate that our model may be a useful tool for exploring the effect of dust on the climate system.

[39] To ensure that the modeled forcing has the correct dependence on ω, we compare it with results from various field campaigns, in the absence of available global observations. Although these field campaigns are local, rather than global, in nature, we verify that the general behavior (as opposed to the absolute magnitude) is similar between them and our modeled results.

[40] *Myhre et al.* [2003] obtain a more strongly negative solar forcing by African dust, by up to a factor of 2, when they used a higher ω rather than the standard value during the Saharan Dust Experiment (SHADE) observational campaign. Our results show a similar response. The TOA shortwave forcing in the $\omega = 0.97$ case is over twice the value of the $\omega = 0.85$ case, suggesting that our model's TOA dependence on ω is realistic. *Haywood et al.* [2003] obtain a surface shortwave forcing 1.6 times the TOA shortwave forcing during SHADE. This is in agreement with our $\omega = 0.97$ model results (surface forcing is 1.8 times TOA forcing), but conflicts with the $\omega = 0.85$ results, where the surface forcing is almost an order of magnitude larger than the TOA forcing, indicating that the $\omega = 0.97$ version of the our model may be more representative of actual dust than the $\omega = 0.85$ version, at least in the region of the SHADE campaign.

[41] *Markowicz et al.* [2003] find that the magnitude of longwave aerosol (including dust) surface forcing was 10 to 25% of the mean diurnal shortwave forcing during the Aerosol Characterization Experiment (ACE-Asia). Our values (28% for $\omega = 0.97$ and 14% for $\omega = 0.85$) are therefore reasonable. For the TOA forcings, *Markowicz et al.* [2003] find that the longwave is 1 to 19% of the shortwave magnitude. *Myhre et al.* [2003] also obtain a TOA longwave forcing much weaker than the shortwave forcing by about a factor of 6 to 7 (14–17%). Our values are
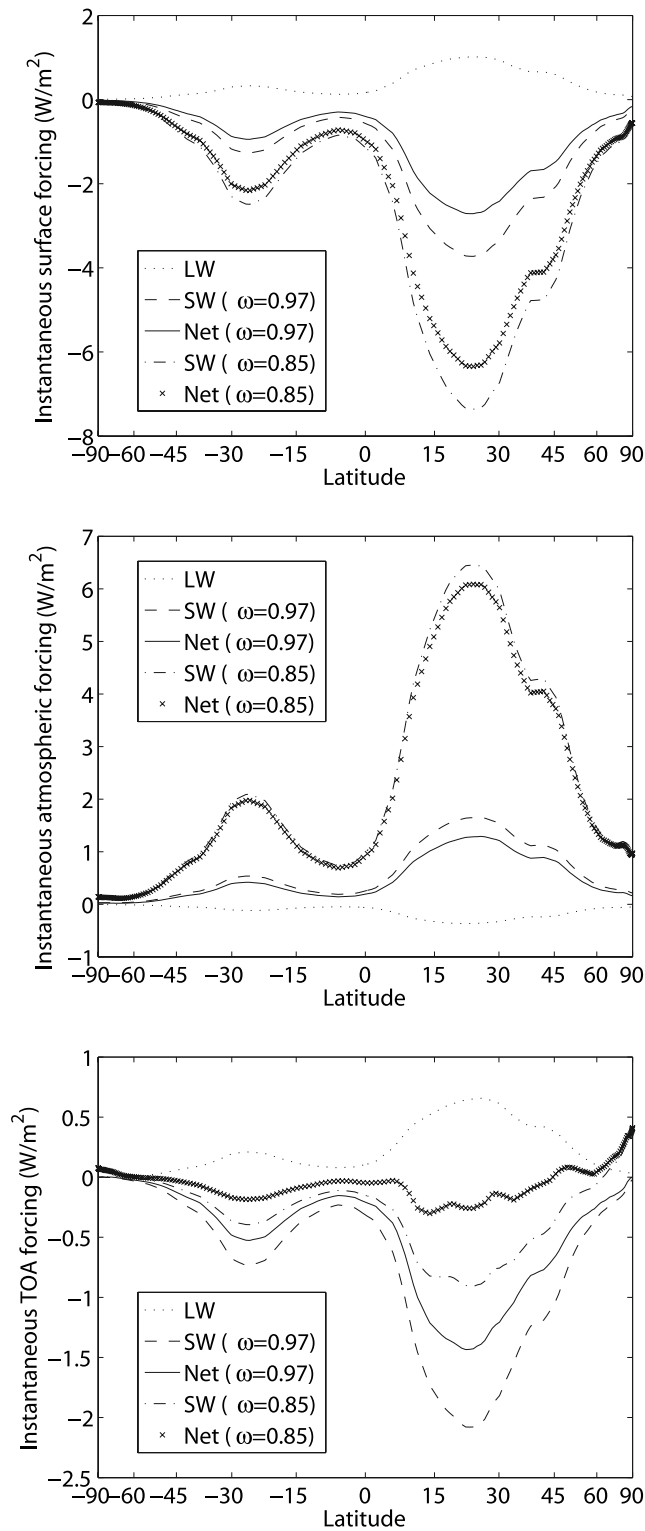
Figure 8. (top) Surface, (middle) atmospheric, and (bottom) TOA longwave, shortwave, and net instantaneous forcing due to dust for the default set of dust optical properties (with $\omega = 0.97$) and the $\omega = 0.85$ case.

higher (32% for $\omega = 0.97$ and 72% for $\omega = 0.85$), though the case of more reflective single scattering albedo is much closer to the *Markowicz et al.* [2003] and *Myhre et al.* [2003] ratios, again suggesting the higher ω value is more in

agreement with recent observations. The lack of global observational coverage makes it impossible to verify the behavior of the simple model in the general sense, but its similarity to local behavior is encouraging, especially since we are interested in the overall system behavior rather than the specific response.

4.2. Climate Response to Forcing

[42] In order to determine the effect of this dust forcing on climate, we next allow the model to adjust to the forcing, reaching a new equilibrium state. In this section, we focus on the $\omega = 0.97$ case, though we present some global average $\omega = 0.85$ results to demonstrate the model's
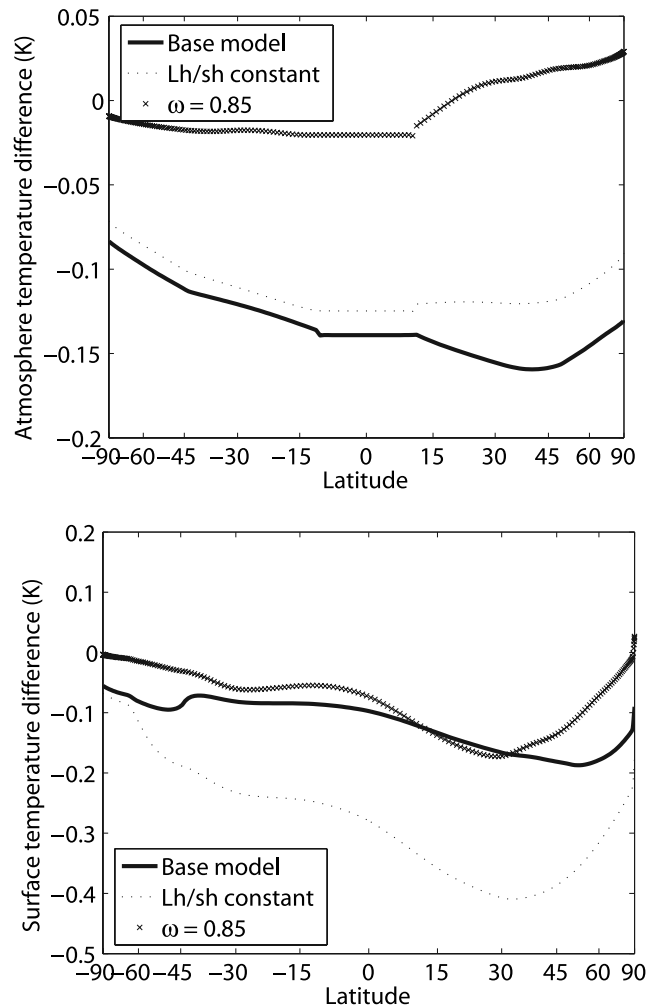
Figure 9. (top) Atmospheric and (bottom) surface temperature change due to dust for three different versions of the model. For the $\omega = 0.97$ case, the thick solid lines correspond to the complete model, while the dotted lines indicate temperature changes in a version of the model where the latent and sensible heat fluxes are specified to be the values obtained from the steady state of the model without dust. Thus these lines show the temperature changes when the air-sea flux feedbacks are omitted. The crosses indicate the $\omega = 0.85$ results for the full version of the model (including air-sea flux feedbacks).
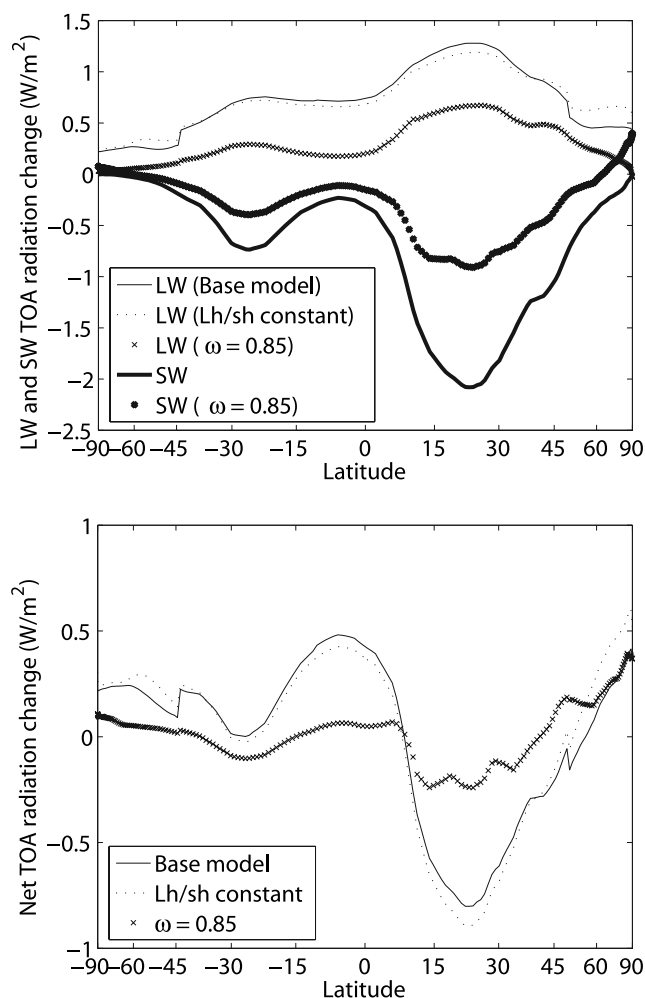
Figure 10. (top) Longwave and shortwave and (bottom) net TOA heating change due to dust. Model versions descriptions are given in the caption for Figure 9. Shortwave results are the same for the base model version and the no latent and sensible heat feedback version, since the shortwave forcing is independent of the climate state.

sensitivity to the choice of ω in Table 3. The figures show results from the $\omega = 0.97$ case, unless otherwise indicated, and we have noted in the text where the results are significantly different between the two cases.

[43] The solid lines in Figure 9 show the resulting temperature changes for the $\omega = 0.97$ case. The atmosphere and surface both cool by over 0.1 K, with the atmospheric cooling slightly more. In the $\omega = 0.85$ case, the atmospheric temperature change is much smaller and becomes positive in middle and high northern latitudes. The surface temperature change is similar to the $\omega = 0.97$ case, except the high latitudes do not cool as much and the cooling peak is closer to the maximum dust forcing latitude, resulting in a smaller global average surface temperature change. Again, we see a decreased dust effect in the lower single scattering albedo case, indicating that temperature changes calculated using the less reflective dust properties may underestimate the effect of dust. In both cases, the flat section of atmospheric

temperature change in the equatorial region is caused by the model's Hadley cell parameterization, which constrains temperature gradients in the tropics. We also determined temperature changes in a version of the model which omits the latent and sensible heating feedback. These results will be discussed in detail later.

[44] Figure 10 shows the steady state TOA radiation budget. The shortwave radiative cooling is focused on the areas of high dust concentration, while the longwave heating (i.e., reduction in outgoing radiation) is more constant with respect to latitude. In essence, the whole planet is cooling in response to the imposed dust forcing. Thus the climate has a net radiative heating near the equator and poles and net cooling in the northern hemisphere region with the highest dust concentration. For the $\omega = 0.85$ case, the TOA budget is similar, though the magnitudes of changes are smaller.

[45] At the surface, the imposed dust forcing can be balanced not only by changes in longwave radiation (solid lines in Figure 11) but also by changes in latent and sensible heating (Figure 12). Most of the compensation for decreased solar heating comes from changes in latent and sensible heat. The surface cools slightly due to the effects of dust, but this cooling results in large reductions of latent and sensible heat transferred from the surface to the atmosphere. In the atmosphere, this reduced latent and sensible heating mostly balances the warming due to solar absorption by dust (not shown).

[46] The decrease in latent and sensible heating is a significant change to the climate system. Globally averaged, sensible heating is reduced by 0.3 W/m², and latent heating is reduced by 0.7 W/m². These values are about 1% of the total fluxes. Reductions are larger in the $\omega = 0.85$ case, since this version experiences larger surface cooling. Similar to our results, *Miller et al.* [2004] obtain a 1.3% reduction in latent heat flux when they include interactive dust in the GISS AGCM [*Miller and Tegen*, 1998]. They also observe a decrease of −0.47 W/m² in sensible heating.

[47] When *Miller et al.* [2004] increase the single scattering albedo, the latent heat flux change becomes more negative, while the sensible heat change becomes positive. In contrast, in our model, both the latent heat and sensible heat changes are less negative with the higher single scattering albedo. This conflicting behavior is addressed more fully by *Shell and Somerville* [2007].

[48] The dotted lines in Figures 9, 10, and 11 show the climate response when the latent and sensible heat fluxes are held constant for the $\omega = 0.97$ case. (They are specified as the values from the steady state of the model without dust.) The surface temperature (Figure 9) decrease is much larger (a maximum of about −0.4 K), while the atmosphere cools slightly less. The TOA budget (Figure 10) does not change much. The longwave effect is merely redistributed slightly, since the longwave heating still must balance the shortwave cooling. However, at the surface (Figure 11), the global average longwave heating must now balance the shortwave cooling by itself, without any compensation by the latent and sensible heat fluxes. (The shortwave cooling is, of course, unchanged, since the model includes no shortwave feedbacks.) Therefore the longwave heating is much larger, as the surface cools more in order to reduce its radiative emission. These results demonstrate that latent and
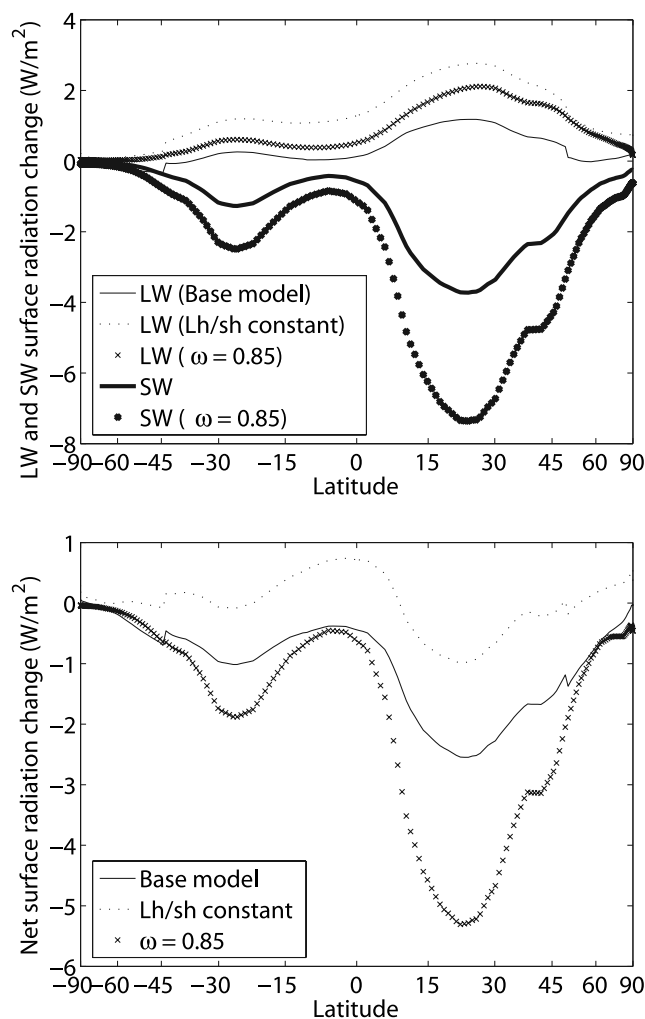
Figure 11. (top) Longwave and shortwave and (bottom) net surface radiative heating change due to dust. Model versions descriptions are given in the caption for Figure 9. Shortwave results are the same for the base model version and the no latent and sensible heat feedback version, since the shortwave forcing is independent of the climate state.

sensible heat fluxes have a large effect on the way climate adjusts to dust forcing.

5. Sensitivity to Dust Optical Depth

[49] One of the largest uncertainties in determining the effect of dust is the magnitude of the atmospheric dust concentration. Recent estimates of dust loading vary by a factor of 4 [*Zender et al.*, 2004]. This large range contributes to uncertainties in dust forcing and climate response. As a starting point, we consider the effect of multiples of the default dust distribution. Future work will explore the uncertainties caused by different estimates of dust distributions, including latitudinal as well as magnitude variations.

[50] Observational studies suggest that local TOA and surface forcings are linear functions of aerosol optical depth [*Weaver et al.*, 2002; *Markowicz et al.*, 2003; *Hsu et al.*, 2000]. Furthermore, experiments using column radiative

transfer models [*Liao and Seinfeld*, 1998] and general circulation models [*Miller et al.*, 2004] show a quasi-linear relationship between the TOA and surface forcings and the dust load or optical thickness. To study the climate response to changes in dust optical depth, we multiplied the specified dust distribution by various constants. In agreement with this previous work, both the longwave and shortwave forcings are approximately linear with respect to dust optical depth. The TOA shortwave forcing at 10 times the present-day dust concentration is 10.5 times the present-day forcing. The longwave forcing is completely linear with respect to optical depth, since the simple longwave parameterization used by this model is linear (see equations (23) and (24) in the auxiliary material).

[51] While the dust forcing is essentially linear with respect to optical depth, the steady state climate response, which cannot be determined from local measurements or single column models, might not be. Figure 13 plots global average temperature and latent heating changes as a function of TOA shortwave, longwave, and total forcing. (Note that for the shortwave and total forcing plots, an increase in dust optical depth corresponds to a more negative forcing.) The dotted lines correspond to an experiment where dust has only a shortwave effect; the dashed lines show results when dust affects only the longwave budget. The solid lines correspond to variations in the total dust amount, affecting both the shortwave and longwave budgets.

[52] The temperature and latent heat changes are all essentially linear with respect to changes in TOA forcing. However, the relationship between the forcing magnitude and climate response varies based on whether longwave or shortwave forcing is applied, as shown by the different slopes of the three lines in Figure 13. Per unit of TOA forcing, the surface (atmospheric) temperature changes by 0.1 (0.2) K when only shortwave forcing is applied, 0.6 (0.7) K when only longwave forcing is applied, and 0.2 (0.3) K when both change simultaneously. Similarly, the latent heat changes by 0.9 W/m² in response to shortwave forcing of 1 W/m², 3.5 W/m² in response to longwave
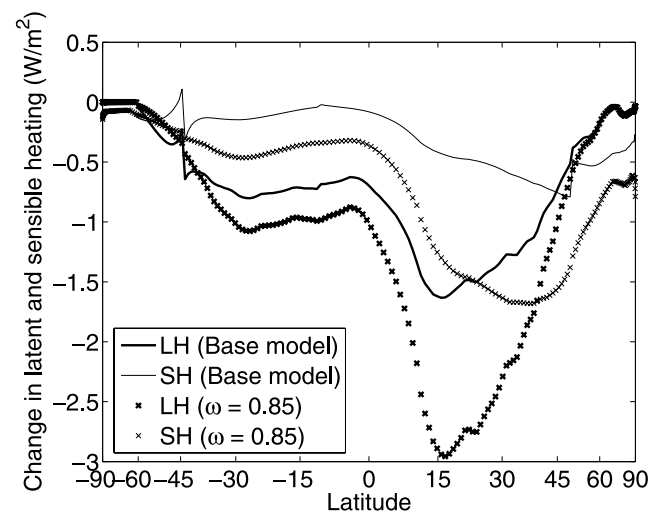
Figure 12. Latent (thick lines) and sensible (thin lines) heating change due to dust radiative forcing. Model versions descriptions are given in the caption for Figure 9.
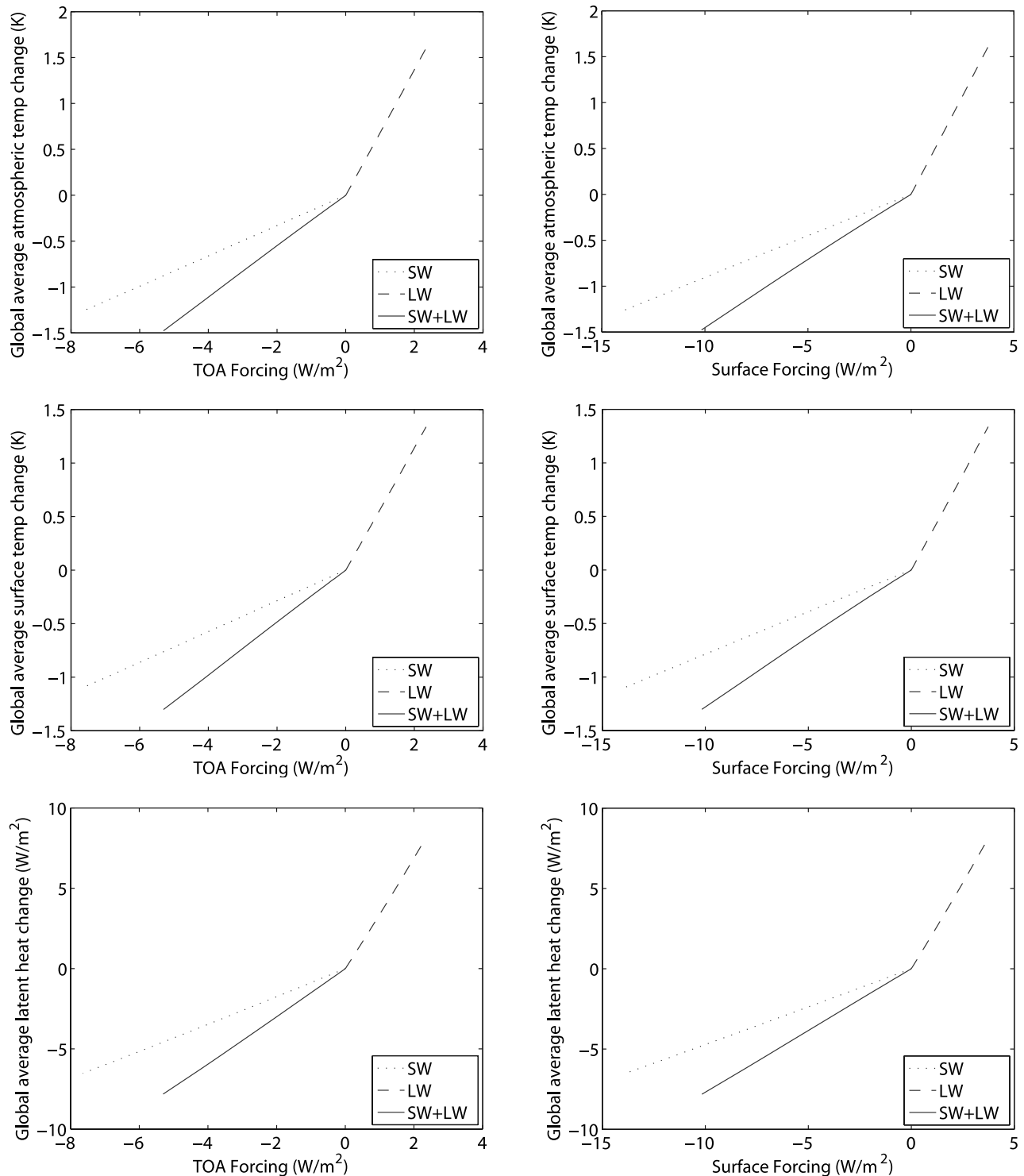
Figure 13. Global average steady state (top) atmospheric and (middle) surface temperature and (bottom) latent heat change as a function of shortwave, longwave, and shortwave plus longwave (left) TOA and (right) surface instantaneous dust forcing.

forcing, and 1.5 W/m² when the forcing is a combination of both.

[53] Thus the type of forcing (i.e., shortwave versus longwave), in addition to the magnitude, is important in determining the temperature change. The magnitude of the climate change response is largest for longwave forcing. That is, for a given change in forcing magnitude, the model produces a larger temperature or latent heat change for longwave heating than for shortwave cooling. The climatic effect of net (shortwave plus longwave) radiative heating

changes lies in between the individual shortwave and long-wave effects. This difference in response to longwave versus shortwave forcings of the same magnitude is related to the different vertical distributions of the forcing. The dust longwave forcing tends to be the same sign for both the atmosphere and surface, while dust shortwave instantaneous forcing is generally negative at the surface and positive for the atmosphere.

[54] The climate response can be approximated as linear for dust concentration changes of an order of magnitude. However, the linear relationship between dust forcing and climate response depends on whether shortwave or long-wave forcing is applied. These experiments demonstrate that the climate response depends not only on the magnitude and sign of the forcing, but also on the type of forcing.

6. Conclusions

[55] We have developed a computationally efficient model for investigating the climate response to direct radiative forcing by atmospheric aerosols. In this paper, we study the effect of the present-day mineral dust concentration on temperature and latent heating. Our model, despite its simplicity, is able to produce results comparable to those obtained from GCM experiments.

[56] In this work, we extend *Shell and Somerville* [2005] to include longwave and shortwave aerosol forcing of the climate system. We have focused on surface temperature, atmospheric temperature, and latent heating as the three main climate variables. Our model is complex enough to resolve these variables while omitting many complicating details, allowing us to focus on a conceptual understanding of the processes and feedbacks involved.

[57] In order to validate our model, we compare our results to those obtained from GCMs for the present-day dust distribution. We also perform a Pinatubo volcanic aerosol simulation to take advantage of the data available from this natural climate experiment. Despite the conceptual simplicity of the model and the idealized nature of the model parameterizations, the present model reproduces the observations and GCM results to a remarkable degree of quantitative correspondence. Indeed, the differences between our forcing and response results and those from observations and GCM experiments is comparable to the discrepancies between the different GCM results. This ability of a tractable theoretical model to replicate the solutions of a complex GCM suggests that our model captures the essential physics and thus can be a valuable guide in interpreting and understanding GCM results.

[58] Using the *Tegen et al.* [1997] dust distribution, we obtain a global average TOA shortwave forcing of -0.73 W/m^2 and longwave forcing of 0.23 W/m^2. At the surface, the shortwave forcing is -1.34 W/m^2, and the longwave forcing is 0.37 W/m^2. Using a lower value for the shortwave single scattering albedo reduces the TOA shortwave forcing by over half, while the surface forcing doubles. For the default ω, dust decreases the global average surface and atmospheric temperatures by about a tenth of a degree K. These temperature changes are smaller in the reduced single scattering albedo simulation. These experi-

ments suggest that previous work which used older (i.e., smaller) values of the dust single scattering albedo may have underestimated the effect of dust.

[59] In response to dust, significant changes occur in the latent heat flux, which decreases by 0.74 W/m^2, a 1% decrease, with a larger change in the smaller single scattering albedo case. The latent heat changes, in turn, may result in other feedbacks not included in this model. For example, a changed hydrologic cycle will alter the distribution of water vapor and clouds, with effects on the longwave and shortwave radiative budgets. In addition, decreased precipitation may increase the dust concentration itself. Reduced rainout of dust will increase the lifetime of dust in the atmosphere, and a drier climate allows for easier uplift of dust. For example, *Miller et al.* [2004] obtain an increase in dust wet deposition lifetime by a few percent, depending on the specific optical properties used, when they include radiatively interactive dust rather than passive dust. These possible feedback are also not included in the model. However, the magnitude of the modeled latent heat change suggests that focusing on the temperature as the sole measure of climate change misses some important climate system changes.

[60] We also explore the climate response to variations in dust concentration, holding other optical properties constant. Increases in dust optical depth result in increases in the magnitude of global average temperature changes. While the modeled TOA forcing is slightly nonlinear with respect to optical depth, it can be approximated as linear for changes less than an order of magnitude, in agreement with GCM results [*Miller et al.*, 2004]. The modeled climate responds almost linearly to changes in dust optical depth. The temperature changes are small enough that they are linear with respect to the forcing, while latent heating is only slightly nonlinear. However, a more realistic model may include feedbacks such that the climate change is more nonlinear.

[61] While the climate responds linearly to changes in the TOA forcing, the slope depends on whether longwave or shortwave forcing is applied. Per unit of aerosol forcing, longwave forcing results in larger temperature and hydro-logical cycle changes than shortwave forcing. These two types of forcing differ in the vertical distribution of radiative changes. Shortwave forcing tends to cool the surface while warming the atmosphere, while longwave forcing warms both the atmosphere and surface. Thus the different climate-forcing relationship between the two types of forcing indicates that the climate response depends on more than the TOA radiative forcing alone. However, changes in aerosol concentration which result in proportional increases in both the longwave and shortwave forcing (such as increases in the overall dust concentration) are linear with respect to forcing. Only when the two forcings have unequal fractional changes will the resulting climate change behave significantly nonlinearly.

[62] Despite its simplicity, our model is able to reproduce a number of results obtained from more complicated models. It has also proven useful in isolating interactions between components, such as the effect that changes in the latent and sensible heat fluxes have on the temperature response. However, many feedbacks and transient effects that may significantly alter the climate response are deliberately not

included in this model. Thus care should be taken when interpreting the results. Keeping this in mind, the model is useful for understand basic interactions between climate components and for suggesting paths of future exploration with GCMs. *Shell and Somerville* [2007] take advantage of the model's speed and realism to explore how the response depends on the dust optical properties.

References

Bluth, G. J. S., S. D. Doiron, C. C. Schnetzler, A. J. Krueger, and L. S. Walter (1992), Global tracking of the SO_2 clouds from the June, 1991 Mount Pinatubo eruptions, *Geophys. Res. Lett.*, 19(2), 151–154.

Budyko, M. I. (1969), The effect of solar radiation variations on the climate of the Earth, *Tellus*, 21, 611–619.

Carlson, T. N., and S. G. Benjamin (1980), Radiative heating rates for Saharan dust, *J. Atmos. Sci.*, 37, 193–213.

Christopher, S. A., J. Wang, Q. Ji, and S. Tsay (2003), Estimation of diurnal shortwave dust aerosol radiative forcing during PRIDE, *J. Geophys. Res.*, 108(D19), 8596, doi:10.1029/2002JD002787.

Claquin, T., M. Schulz, Y. Balkanski, and O. Boucher (1998), Uncertainties in assessing radiative forcing by mineral dust, *Tellus, Ser. B*, 50, 491–505.

Claquin, T., et al. (2003), Radiative forcing of climate by ice-age atmospheric dust, *Clim. Dyn.*, 20, 193–202.

Clarke, A. D., et al. (2004), Size distributions and mixtures of dust and black carbon aerosol in Asian outflow: Physiochemistry and optical properties, *J. Geophys. Res.*, 109, D15S09, doi:10.1029/2003JD004378.

Coakley, J. A., and R. D. Cess (1985), Response of the NCAR Community Climate Model to the radiative forcing by the naturally occurring tropospheric aerosol, *J. Atmos. Sci.*, 42(16), 1677–1692.

Dutton, E. G., and J. R. Christy (1992), Solar radiative forcing at selected locations and evidence for global lower tropospheric cooling following the eruptions of El Chichon and Pinatubo, *Geophys. Res. Lett.*, 19(23), 2313–2316.

Hansen, J., I. Fung, A. Lacis, D. Rind, S. Lebedeff, R. Ruedy, G. Russell, and P. Stone (1988), Global climate changes at forecast by Goddard Institute for space studies three-dimensional model, *J. Geophys. Res.*, 93, 9341–9364.

Hansen, J., M. Sato, and R. Ruedy (1997), Radiative forcing and climate response, *J. Geophys. Res.*, 102, 6831–6864.

Hansen, J., et al. (2002), Climate forcings in Goddard Institute for Space Studies SI2000 simulations, *J. Geophys. Res.*, 107(D18), 4347, doi:10.1029/2001JD001143.

Haywood, J., P. Francis, S. Osborne, M. Glew, N. Loeb, E. Highwood, D. Tanr, G. Myhre, P. Formenti, and E. Hirst (2003), Radiative properties and direct radiative effect of Saharan dust measured by the C-130 aircraft during SHADE: 1 Solar spectrum, *J. Geophys. Res.*, 108(D18), 8577, doi:10.1029/2002JD002687.

Held, I. M., and A. Y. Hou (1980), Nonlinear axially symmetric circulations in a nearly inviscid atmosphere, *J. Atmos. Sci.*, 37, 515–533.

Hsu, N. C., J. R. Herman, and C. Weaver (2000), Determination of radiative forcing of Saharan dust using combined TOMS and ERBE data, *J. Geophys. Res.*, 105, 20,649–20,661.

Intergovernmental Panel on Climate Change (IPCC) (2001), *Climate Change 2001: The Scientific Basis. Contribution of Working Group I to the Third Assessment Report of the Intergovernmental Panel on Climate Change*, edited by J. T. Houghton et al., 881 pp., Cambridge Univ. Press, New York.

Jacobson, M. Z. (2001), Global direct radiative forcing due to multicomponent anthropogenic and natural aerosols, *J. Geophys. Res.*, 106, 1551–1568.

Jones, P., and K. Briffa (1992), Global surface air temperature variations over the twentieth century. part 1: Spatial, temporal, and seasonal details., *Holocene*, 2, 165–179.

Joseph, J. H., W. J. Wiscombe, and J. A. Weinman (1976), The delta-Eddington approximation for radiative flux transfer, *J. Atmos. Sci.*, 33, 2452–2459.

Kaufman, Y. J., D. Tanré, O. Dubovik, A. Karnieli, and L. A. Remer (2001), Absorption of sunlight by dust as inferred from satellite and ground-based remote sensing, *Geophys. Res. Lett.*, 28(8), 1479–1482.

Kirchner, I., G. L. Stenchikov, H.-F. Graf, A. Robock, and J. C. Antuña (1999), Climate model simulation of winter warming and summer cooling following the 1991 Mount Pinatubo volcanic eruption, *J. Geophys. Res.*, 104, 19,039–19,056.

Koepke, P., M. Hess, I. Schult, and E. Shettle (1997), Global aerosol data set, *Tech. Rep. 243*, Max-Planck-Inst. für Meteorol., Hamburg, Germany.

Lacis, A. A., and M. I. Mishchenko (1995), Climate forcing, climate sensitivity, and climate response: A radiative modeling perspective on atmospheric aerosols, in *Aerosol Forcing of Climate*, edited by R. Charlson and J. Heintzenberg, pp. 11–42, John Wiley, Hoboken, N. J.

Liao, H., and J. H. Seinfeld (1998), Radiative forcing by mineral dust aerosols: Sensitivity to key variables, *J. Geophys. Res.*, 103, 31,637–31,645.

Liou, K. N. (2002), *An Introduction to Atmospheric Radiation*, 2nd ed., 583 pp., Elsevier, New York.

Mahowald, N. M., and C. Luo (2003), A less dusty future?, *Geophys. Res. Lett.*, 30(17), 1903, doi:10.1029/2003GL017880.

Mahowald, N. M., G. D. R. Rivera, and C. Luo (2004), Comment on "Relative importance of climate and land use in determining present and future global soil dust emission" by I. Tegen et al., *Geophys. Res. Lett.*, 31, L24105, doi:10.1029/2004GL021272.

Markowicz, K. M., P. J. Flatau, A. M. Vogelmann, P. K. Quinn, and E. J. Welton (2003), Clear-sky infrared aerosol radiative forcing at the surface and the top of the atmosphere, *Q. J. R. Meteorol. Soc.*, 129(594), 2927–2947.

Miller, R. L., and I. Tegen (1998), Climate response to soil dust aerosols, *J. Clim.*, 11, 3247–3267.

Miller, R. L., and I. Tegen (1999), Radiative forcing of a tropical direct circulation by soil dust aerosols., *J. Atmos. Sci.*, 56, 2403–2433.

Miller, R. L., I. Tegen, and J. Perlwitz (2004), Surface radiative forcing by soil dust aerosols and the hydrologic cycle, *J. Geophys. Res.*, 109, D04203, doi:10.1029/2003JD004085.

Miller, R. L., et al. (2006), Mineral dust aerosols in the NASA Goddard Institute for Space Sciences ModelE atmospheric general circulation model, *J. Geophys. Res.*, 111, D06208, doi:10.1029/2005JD005796.

Myhre, G., and F. Stordal (2001), Global sensitivity experiments of the radiative forcing due to mineral aerosols, *J. Geophys. Res.*, 106, 18,193–18,204.

Myhre, G., A. Grini, J. M. Haywood, F. Stordal, B. Chatenet, D. Tanr, J. K. Sundet, and I. S. A. Isaksen (2003), Modeling the radiative impact of mineral dust during the Saharan Dust Experiment (SHADE) campaign, *J. Geophys. Res.*, 108(D18), 8579, doi:10.1029/2002JD002566.

Oman, L., A. Robock, G. Stenchikov, G. A. Schmidt, and R. Ruedy (2005), Climatic response to high-latitude volcanic eruptions, *J. Geophys. Res.*, 110, D13103, doi:10.1029/2004JD005487.

Perlwitz, J., I. Tegen, and R. L. Miller (2001), Interactive soil dust aerosol model in the GISS GCM: 1. Sensitivity of the soil dust cycle to radiative properties of soil dust aerosols, *J. Geophys. Res.*, 106, 18,167–18,192.

Robock, A., and Y. Liu (1994), The volcanic signal in Goddard Institute for Space Studies three-dimensional model simulations, *J. Clim.*, 7(1), 44–55.

Robock, A., and J. Mao (1995), The volcanic signal in surface temperature observations, *J. Clim.*, 8, 1086–1103.

Sato, M., J. Hansen, M. P. McCormick, and J. Pollack (1993), Stratospheric aerosol optical depth, *J. Geophys. Res.*, 98, 22,987–22,994.

Sellers, W. D. (1969), A global climatic model based on the energy balance of the Earth-atmosphere system, *J. Appl. Meteorol.*, 8, 392–400.

Shell, K. M., and R. C. J. Somerville (2005), A generalized energy balance climate model with parameterized dynamics and diabatic heating, *J. Clim.*, 18, 1753–1772.

Shell, K. M., and R. C. J. Somerville (2007), Sensitivity of climate forcing and response to dust optical properties in an idealized model, *J. Geophys. Res.*, doi:10.1029/2006JD007198, in press.

Soden, B. J., R. T. Wetherald, G. L. Stenchikov, and A. Robock (2002), Global cooling following the eruption of Mt. Pinatubo: A test of climate feedback by water vapor, *Science*, 296, 727–730.

Sokolik, I. N., and O. B. Toon (1996), Direct radiative forcing by anthropogenic airborne mineral aerosols, *Nature*, 381, 681–683.

Sokolik, I., A. Andronova, and T. Johnson (1993), Complex refractive index of atmospheric dust aerosols, *Atmos. Environ., Part A*, 27, 2495–2502.

Stenchikov, G. L., I. Kirchner, A. Robock, H.-F. Graf, J. C. Antuña, R. G. Grainger, A. Lambert, and L. Thomason (1998), Radiative forcing from the 1991 Mount Pinatubo volcanic eruption, *J. Geophys. Res.*, 103, 13,837–13,857.

Stone, P. H. (1974), The meridional variation of the eddy heat fluzes by baroclinic waves and their parameterization, *J. Atmos. Sci.*, 31, 444–456.

Stone, P. H. (1978), Baroclinic adjustment, *J. Atmos. Sci.*, 35, 561–571.

Tegen, I., and I. Fung (1994), Modeling of mineral dust in the atmosphere: Sources, transport, and optical thickness, *J. Geophys. Res.*, 99, 22,897–22,914.

Tegen, I., and I. Fung (1995), Contribution to the atmospheric mineral aerosol load from land surface modification, *J. Geophys. Res.*, 100, 18,707–18,726.

Tegen, I., and A. A. Lacis (1996), Modelling of particle size distribution and its influence on the radiative properties of mineral dust aerosol, *J. Geophys. Res.*, 101, 19,237–19,244.

Tegen, I., A. A. Lacis, and I. Fung (1996), The influence on climate forcing of mineral aerosols from disturbed soils, *Nature*, 380, 419–422.

Tegen, I., P. Hollrig, M. Chin, I. Fung, D. Jacob, and J. Penner (1997), Contribution of different aerosol species to the global aerosol extinction optical thickness: Estimates from model results, *J. Geophys. Res.*, 102, 23,895–23,915.

Tegen, I., S. P. Harrison, K. Kohfeld, I. C. Prentice, M. Coe, and M. Heimann (2002), Impact of vegetation and preferential source areas on global dust aerosol: Results from a model study, *J. Geophys. Res.*, 107(D21), 4576, doi:10.1029/2001JD000963.

Tegen, I., M. Werner, S. P. Harrison, and K. E. Kohfeld (2004a), Relative importance of climate and land use in determining present and future global soil dust emission, *Geophys. Res. Lett.*, 31, L05105, doi:10.1029/2003GL019216.

Tegen, I., M. Werner, S. P. Harrison, and K. E. Kohfeld (2004b), Reply to comment by N. M. Mahowald et al. on "Relative importance of climate and land use in determining present and future global soil dust emission," *Geophys. Res. Lett.*, 31, L24106, doi:10.1029/2004GL021560.

Thompson, S., and D. Pollard (1997), Greenland and Antarctic mass balances for present and doubled CO_2 from the GENESIS version-2 global climate model, *J. Clim.*, 10, 871–900.

Trochkine, D., Y. Iwasaka, A. Matsuki, M. Yamada, Y.-S. Kim, T. Nagatani, D. Zhang, G.-Y. Shi, and Z. Shen (2003), Mineral aerosol particles collected in Dunhuang, China, and their comparison with chemically modified particles collected over Japan, *J. Geophys. Res.*, 108(D23), 8642, doi:10.1029/2002JD003268.

Wang, J., S. A. Christopher, J. S. Reid, H. Maring, D. Savoie, B. N. Holben, J. M. Livingston, P. B. Russell, and S. Yang (2003), GOES 8 retrieval of dust aerosol optical thickness over the Atlantic Ocean during PRIDE, *J. Geophys. Res.*, 108(D19), 8595, doi:10.1029/2002JD002494.

Weaver, C. J., P. Ginoux, N. C. Hsu, M. D. Chou, and J. Joiner (2002), Radiative forcing of Saharan dust: GOCART model simulations compared with ERBE data, *J. Atmos. Sci.*, 59, 736–747.

Woodward, S. (2001), Modeling the atmospheric life cycle and radiative impact of mineral dust in the Hadley Centre climate model, *J. Geophys. Res.*, 106, 18,155–18,166.

Yoshioka, M., N. M. Mahowald, A. J. Conley, W. D. Collins, D. W. Fillmore, C. S. Zender, and D. B. Coleman (2006), Impact of desert dust radiative forcing on Sahel precipitation: Relative importance of dust compared to sea surface temperature variations, vegetation changes, and greenhouse gas arming, *J. Clim.*, in press.

Zender, C. S., R. Miller, and I. Tegen (2004), Quantifying mineral dust mass budgets: Terminology, constraints, and current estimates, *Eos Trans. AGU*, 85(48), 509.

————————————

K. M. Shell, College of Oceanic and Atmospheric Sciences, 104 COAS Admin. Bldg., Corvallis, OR 97331–5503, USA. (kshell@coas.oregonstate.edu)

R. C. J. Somerville, Scripps Institution of Oceanography, University of California, San Diego, 9500 Gilman Drive, Dept. 0224, La Jolla, CA 92093, USA.